PHILIPPINE JOURNAL OF
Ophthalmology
VOL. 31 • NO. 1 JANUARY - JUNE 2006

ORIGINAL ARTICLE

Correlation of ocular ultrasonography with histopathologic findings in intraocular retinoblastoma

Romeo B. Espiritu, MD
Eric G. Valera, MD
Arnel A. de Jesus, MD
Yasmyne C. Ronquillo, MD
Gary V. Mercado, MD

Department of Ophthalmology and Visual Sciences
University of the Philippines-Philippine General Hospital
Manila, Philippines

ABSTRACT

Objective

This study correlated the patterns of ocular B- and A-scans of intraocular retinoblastoma (RB) with corresponding histopathology sections. It aimed to establish a more objective basis for determining intraocular retinoblastoma by ultrasonography (UTZ) and to determine the degree of malignancy and viability of the tumor cells.

Methods

New cases of retinoblastoma seen at the University of the Philippines–Philippine General Hospital (UP–PGH) from January 1994 to December 2003 were reviewed. Included were patients who underwent enucleation and whose eyeballs were processed at the UP Institute of Ophthalmology. Those with good quality ocular ultrasonographs (UTZ) and clear matching histopathologic sections were finally selected. Findings were correlated and analyzed.

Results

Retinoblastoma (RB) showed multiplicity of lesions on UTZ corresponding to multiple lesions on histopathology. The following characteristic patterns were seen:

Very malignant RB or pseudorosettes: fine, grainy densities on B-scan with short to medium broad spikes on A-scan ("V-W" pattern).

Moderate differentiation with moderate necrosis and early calcific plaques: fine, dense grainy opacities on B-scan with multiple thin, high spikes admixed with tall, broad spikes of calcium deposits on A-scan.

Well-differentiated RB with compact viable cells and no necrosis: large, white densities on B-scan with an initial high spike and high internal reflectivity, sometimes "plateauing," on A-scan with no calcific deposits.

Complete tumor necrosis with calcific plaques: echolucent space with dense, white, plaque-like opacities on B-scan; flat or low spikes mixed with tall, broad spikes corresponding to calcium plaques on A-scan.

Correspondence to
Romeo B. Espiritu, MD
Department of Ophthalmology and Visual Sciences
University of the Philippines-Philippine General Hospital
Taft Avenue, Ermita
1000 Manila, Philippines
Telephone : +63-2-3022491

Presented at the second Joint Meeting of the Philippine Academy of Ophthalmology (PAO) and the Singapore Eye Research Institute (SERI) on July 30, 2005 in Manila.

The authors have no proprietary or financial interest in any product used or cited in this study.

Keywords: *Retinoblastoma, Histopathology, Ocular ultrasonography*

PHILIPP J OPHTHALMOL 2006; 31(1): 14-21

Normal vitreous, serous subretinal fluid, or recent hemorrhage: echolucent area on B-scan with flat or low spikes on A-scan.

Conclusion

The three most frequent findings in intraocular retinoblastoma were calcific plaques with liquefaction necrosis, multiplicity of lesions, and pseudorosettes. Ocular ultrasound of retinoblastoma showed good histopathologic correlation.

RETINOBLASTOMA is the most common primary intraocular tumor in childhood. A 35-year (1967 to 2001) epidemiologic survey of retinoblastoma at a tertiary referral center in the Philippines[1] showed a high incidence (237 per 100,000 eye cases) despite advances in medical technology and therapy.

Ocular ultrasonography (UTZ) usually provides a fairly accurate diagnostic evidence using echoes to describe intraocular structures, especially in hazy or opaque ocular media.[2, 3, 4] However, echo patterns in retinoblastoma are widely varied and may be misinterpreted for other intraocular disease entities.[5] Local studies have shown a 16% misdiagnosis of 48 enucleated eyeballs[6, 7]—8 false positives and 1 false negative. This can result in missed or delayed diagnosis of the tumor, or in extreme cases, the enucleation of an eye with benign lesions with consequent lifetime cosmetic problems and complications associated with the use of an ocular prosthesis.

There has been no detailed study describing and directly correlating specific echo patterns in B- and A-scans of retinoblastoma with explicit anatomic tissue structures demonstrated by matching histopathologic features. The histopathology has been utilized mainly to confirm the diagnosis.[8] This study compared the echo patterns in ocular vector B-scans and A-scans of retinoblastoma in eyes that underwent enucleation with its corresponding histopathologic features. It aimed to establish a more objective and accurate basis for interpretation of retinoblastoma via UTZ. We also determined the nature, extent, degree of malignancy, viability, and other intraocular lesions, such as calcification, tumor necrosis, areas of hemorrhage, total retinal detachment with tumor, and choroidal extension, as seen in retinoblastoma.

METHODOLOGY

New cases of retinoblastoma seen from January 1994 to December 2003 at the University of the Philippines-Philippine General Hospital (UP-PGH) were reviewed. Included were patients who underwent enucleation and whose eyeballs were processed at the pathology section of the Institute of Ophthalmology, University of the Philippines Manila (n = 122). The eyeballs were preserved overnight in 10% formalin solution and calottes were cut in the horizontal meridian, except in cases where it was necessary to cut in another meridian to highlight a special lesion. The sliced paraffin blocks were stained in Hematoxylin–Eosin (H & E) dye. Repeat sections of the paraffin blocks were done for unacceptable slides. Good quality ultrasonographic printouts were obtained with the Alcon Ultra Scan 2 D 20 MHz with depth of 30 mm and sensitivity or gain of 80. A combined B- and A-scan record was made. Good matching clear histopathology and UTZ sections were chosen (n = 27) by one of the investigators (RBE). All others were excluded.

A retina specialist (RBE) reevaluated the echo patterns in the UTZ while an ophthalmic pathologist identified and correlated areas of interest. The UTZ printouts (combined B- and A-scans) with the corresponding eyeball sections and high magnification photomicrographs (computed tomography) were arranged side by side for easy comparison as shown in Figure 1. Pertinent data (age, sex, presenting symptoms) and histopathologic diagnosis were also included. Areas of interest such as detached retina, overlying vitreous, the retinoblastoma tumor, subretinal serous fluid, and the degree of malignancy and viability of the tumor also were included (Figures 2 to 7, 9 to 13). Demographic and clinical data were correlated and analyzed.

RESULTS

Twenty-seven enucleated eyeballs from 25 patients were included in this study. Two patients had both eyes enucleated. There were 16 males and 9 females with mean age of 21.75 $\pm$ 16 months. The youngest was 2.5 months and the oldest 5 years old. In classifying the extent of retinoblastoma, we adopted our modified system of classification[12] as follows:

Stage 1 – Intraocular (confined to the retina)
- Tumor < 1/2 of retinal surface
- Tumor > 1/2 of retinal surface

Stage 2 – Far advanced (tumor extends to other parts of the eyeball)

Stage 3 – Extraocular and/or metastatic

The most common clinical presentation was leukocoria (19 cases), followed by congestive glaucoma (3), lid

Table 1. **Histopathologic findings in 27 eyeballs.**

Histopathology	Number	Percent
Necrosis	26	96
Pseudorosettes	20	73
Calcific deposits	17	62
Hemorrhages: Subretinal, intratumor, vitreous	7	25
Choroidal extension	6	24
True rosettes	4	17

swelling (2), and esotropia, ciliary staphyloma, and early atrophia bulbi (1 each). Almost 60% (16) were enucleated at stage 2 retinoblastoma and 40% (11) at stage 1. Pearson's correlation coefficient showed a positive but insignificant relationship (r = 0.3) between gender and the preoperative clinical staging of retinoblastoma.

Most of the tumors (23) were undifferentiated. The most prominent histologic features were necrosis, pseudorosettes, and calcific plaques (Table 1).

Each histologic lesion showed characteristic B- and A-scan patterns. Highly undifferentiated malignant cases (pseudorosettes) showed fine, grainy densities on B-scan and short to medium broad spikes ("V–W" pattern)[8, 9] located in the middle of the vertical Y axis of the A-scan (Figure 2). Moderately differentiated or less undifferentiated cases with moderate necrosis and early calcification showed denser grains on B-scan and multiple, high, thin spikes interspersed with a few high, broad spikes reflecting early calcium plaques on A-scan (Figure 3). Well-differentiated compact viable tumor cells showed a white, dense mass on B-scan and initial high spike with very high internal reflectivity or even plateauing on A-scan and no calcific deposits (Figure 4). Complete tumor necrosis or liquefaction was seen as echolucent areas on B-scan and flat or low spikes on A-scan (Figure 5). Benign retinoblastoma—often called retinoma, regressed retinoblastoma, retinal dysplasia or immature retinal rosettes—is controversial and will not be discussed extensively. It is included for completeness and because the eyes were clinically diagnosed as retinoblastoma preoperatively. B-scan showed fine densities with complete retinal detachment and A-scan showed multiple thin, high spikes with no evidence of calcification (Figure 6).

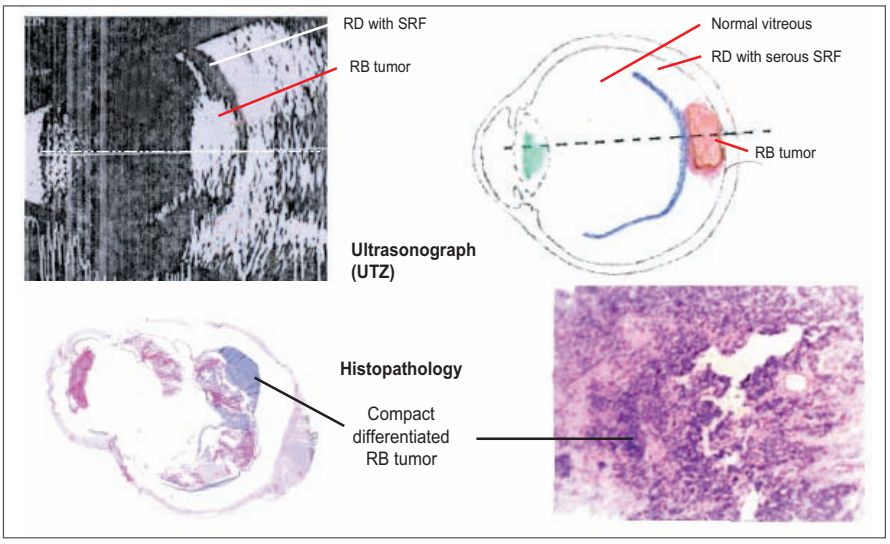

Figure 1. Correlating UTZ and histopathology. Red lines point to retinoblastoma (RB) on B-scan and corresponding A-scan. Black lines point to histopathology of tumor.

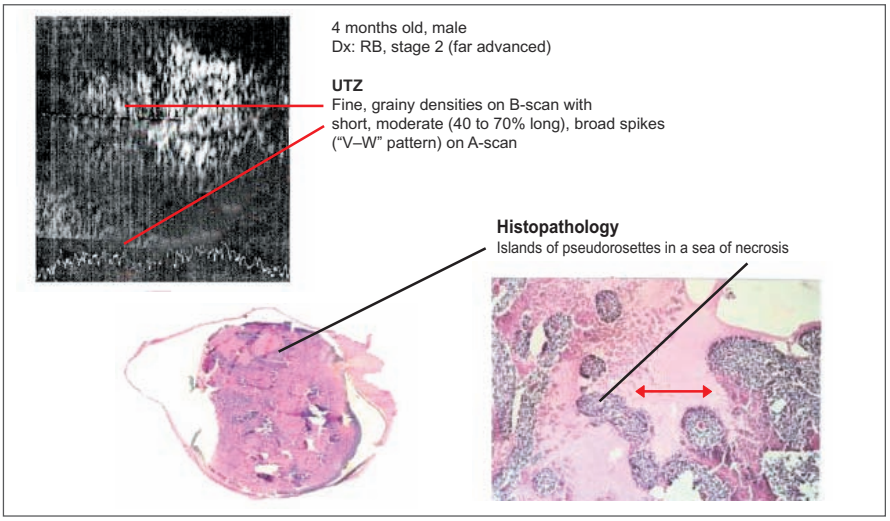

Figure 2. Pseudorosettes in very malignant retinoblastoma (RD) and moderate necrosis.

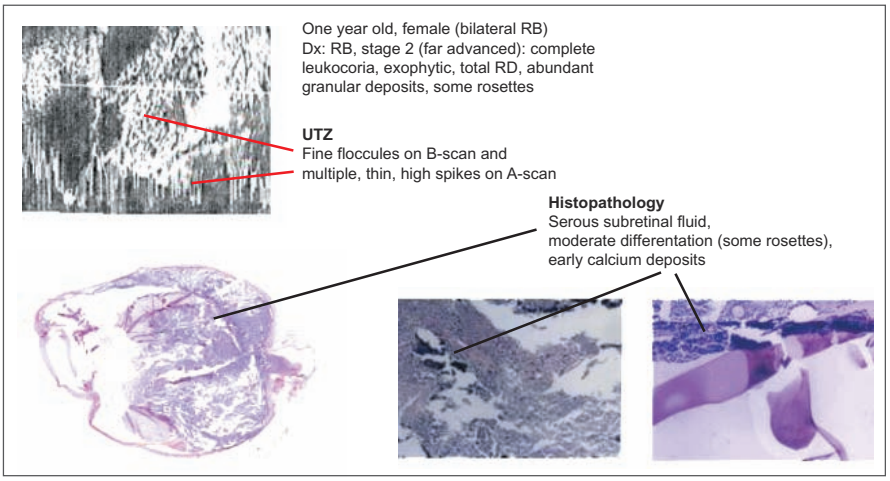

Figure 3. Retinoblastoma (RB) with moderate differentiation, mild necrosis, and early calcium deposits.

Calcific plaques were seen as large dense white nodules on B-scan and high broad spikes on A-scan and with associated prominent areas of echolucent liquefaction necrosis (Figure 7). The ultrasound patterns of the normal vitreous, serous subretinal fluid, and fresh hemorrhage were the same as those of liquefaction necrosis (Figures 9, 10, 11). Choroidal extension of the tumor was manifested as thickened, dense choroid with high internal reflectivity (Figure 12). The typical eyeball lesion of total retinal detachment infiltrated by tumor and with serous subretinal fluid or subretinal hemorrhage is shown in Figure 13. The internal reflectivity depends on the degree of differentiation and viability of the tumor.

Retinoblastoma showed multiple lesions on histopathology (Table 1), as well as on UTZ (Figure 14). This is helpful in differentiating it from single homogenous lesions such as endogenous endophthalmitis or vitreous hemorrhage (Figure 15).

DISCUSSION

An analysis of the histopathologic findings of the retinoblastoma cases studied showed that necrosis, pseudorosettes, and calcific deposits were the most frequent findings (Table 1). Less common were hemorrhages, which may be subretinal, intratumoral or vitreous, choroidal extension, and true rosettes. All of these findings showed corresponding UTZ patterns.

Retinoblastoma exhibited five characteristic UTZ patterns depending on the degree of differentiation—from most malignant (pseudorosettes) to benign (retinoma or retinal dysplasia)—varying cell density, compactness, and viability.

Pseudorosettes or most malignant RB (Figure 2)

The pseudorosettes are seen as malignant cells surrounding a retinal vessel forming round and/or

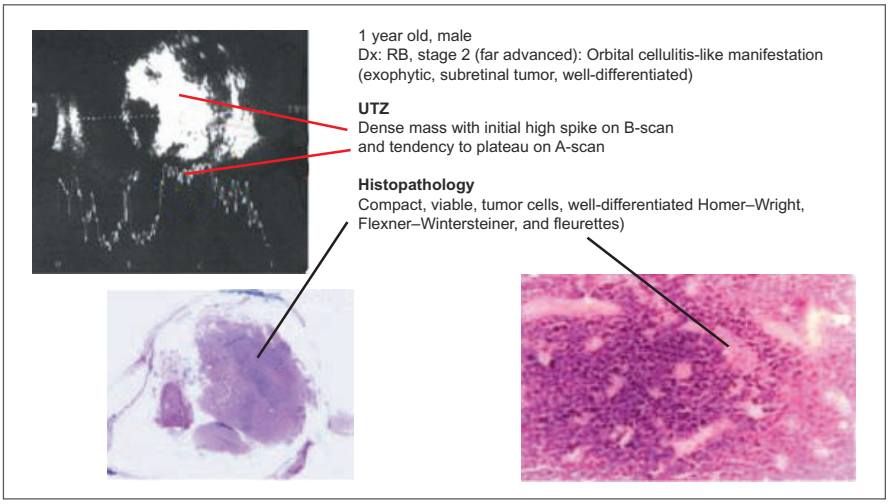

Figure 4. Retinoblastoma (RB) with compact well-differentiated malignancy and no necrosis.

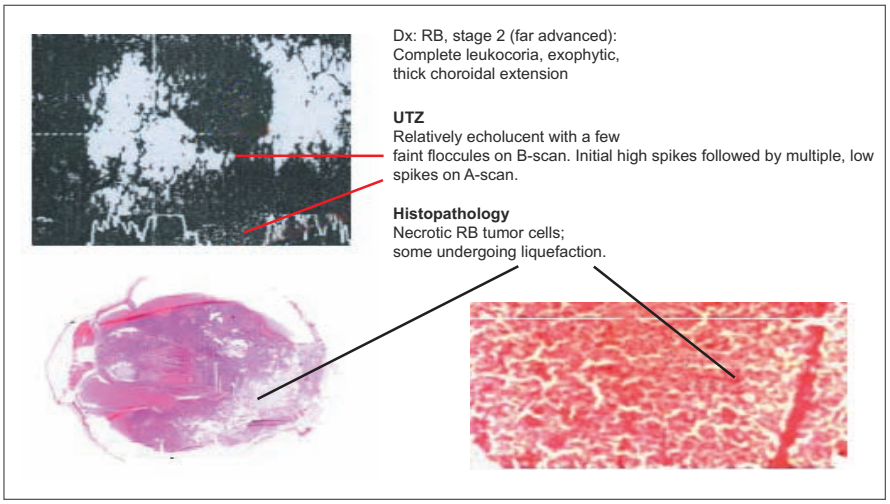

Figure 5. Retinoblastoma (RB) with complete tumor necrosis and calcific plaques.

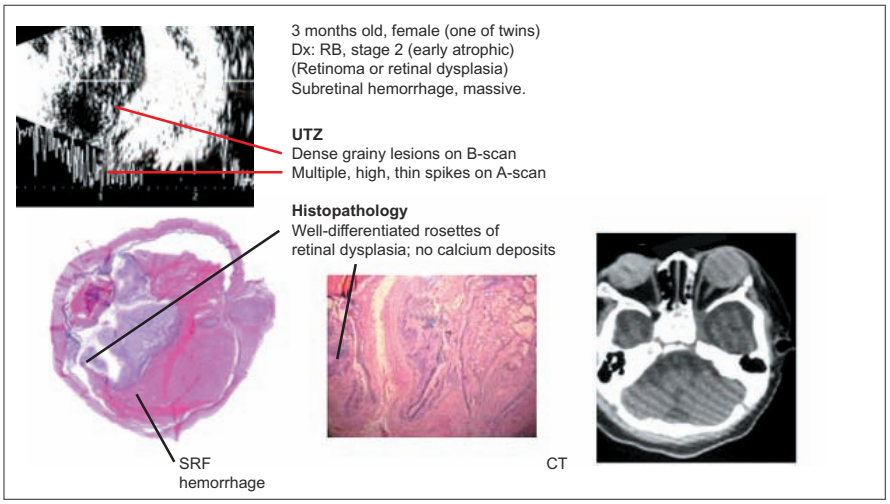

Figure 6. Benign retinoblastoma (RB) — retinoma, regressed retinoblastoma, retinal dysplasia (immature retina with rosettes and loose glial extracellular tissue).

elongated islands in a "sea of necrosis." The B-scan shows fine, grainy densities and the A-scan a typical "V-W pattern" of spikes that are short to medium in length, broad in thickness, and located at the middle portion of the scan. The spikes are not tall, indicating less dense and less compact cells due to rapid cell division. The spikes are broad, reflecting the wide area of necrosis forming the downward slope of the V pattern. The V does not reach the bottom because liquefaction necrosis is not yet complete and suspended necrotic particles are still present on histopathology, producing a low but not zero reflectivity. Pseudorosettes are more frequent in the endophytic type of retinoblastoma where the vitreous is avascular, in contrast to the exophytic type that grows toward the vascular choroid.

Moderate differentiation and moderate necrosis (Figure 3)

The cell types are more differentiated, compact, and viable—Homer-Wright and Flexer-Wintersteiner varieties. Some rosettes are present. The B-scan shows small dense floccules closely grouped. The A-scan shows thin and high spikes; the upward limb of the spike is tall and long, indicating that the cells are more dense and compact; the downward limb of the spikes is also long, indicating a large difference in density between cell groups and extracellular fluid. This difference is one of the factors that determine the height of the spike.[10] True rosettes are also denser than pseudorosettes. Occasional high, slightly broader spikes are seen, corresponding to early calcium plaques and early necrosis. This feature is not specific to retinoblastoma as other intraocular lesions can produce this pattern (Figure 15).

Well-differentiated compact viable tumor (Figure 4)

The B-scan shows a dense, almost uniform mass. The A-scan shows a characteristic but nonspecific feature, initial high spike followed by flattening at the top (plateauing). Histopathologic correlation shows well-differentiated tumor cells (Homer-Wright, Flexner-Wintersteiner rosettes, and fleurettes), which are compactly arranged and viable, and absence of necrosis or calcium.

Complete tumor necrosis or liquefaction (Figure 5)

Although previously referred to as cystic,[11] retinoblastoma has no true cysts. The B-scan shows an area of echolucency or transparency (zero reflectivity). The A-scan shows a flat or low spike, reflecting absent or weak echoes.

Benign retinoblastoma (retinoma or retinal dysplasia) (Figure 6)

Included here for completeness, 2 retinal dysplasia cases (9%) were diagnosed preoperatively as intraocular retinoblastoma. B-scan shows multiple, small, grainy densities similar to moderately differentiated RB (Figure 3). A-scan shows multiple, thin, high spikes. Absense of broad, high spikes reflecting calcium deposits, absence of total retinal detachment with chronic subretinal hemorrhage, and absence of necrosis are important findings differentiating this condition from true retinoblastoma.

Calcific plaques (Figure 7)

Calcific plaques were seen in 62% of the cases studied. In retinoblastoma, the calcium deposits are secondary to necrosis. The B-scan shows dense, white plaques, either solitary or multiple, and associated with areas of necrosis. By lowering the sensitivity of the UTZ, the plaques are better seen with shadowing (Figure 8).

Normal vitreous (Figure 9)

The normal vitreous has zero or very low reflectivity. It is echolucent on B-scan and has flat or very low spikes on A-scan. The vitreous collagen fibrils (vitrein) are smaller than the resolving power of the ultrasonograph used (200 um); they can not reflect back sound waves. When the fibrils break up on vitreous liquefaction (a colloidal gel–sol conversion) and form clumps or when cells (red blood cells, pus cells, tumor cells, etc.) invade the vitreous, the vitreous then becomes visible.

Serous subretinal fluid (SRF) (Figure 10)

Serous subretinal fluid, composed mainly of fluid exudate and similar to normal vitreous, has zero or very low reflectivity. On B-scan, it appears echolucent and situated behind the detached retina seen as a line membrane or as a single, high spike on A-scan.

Fresh subretinal hemorrhage (Figure 11)

A recent subretinal hemorrhage shows echolucency, indicating that the red blood cells are still intact, loose, and smaller than the resolving power of the ultrasonograph (7 um v. 200 um). On histopathologic section, distinct intact red blood cells are seen on high power magnification. In chronic subretinal hemorrhage, the red blood cells form clumps with fibrin clots; as a result, they become reflective and visible (Figure 6).

Choroidal extension (Figure 12)

The choroidal involvement in retinoblastoma is the result of exophytic growth of the tumor. On UTZ, the retina-choroid-sclera complex, or the retina alone, may be totally detached with SRF exudates or subretinal hemorrhage. The choroid shows a diffuse or localized, dense mass on B-scan and high reflectivity on A-scan. The tumor cells show moderate differentiation on histopathology. No necrosis is present because of the high vascularity and increased blood flow in the choroid.

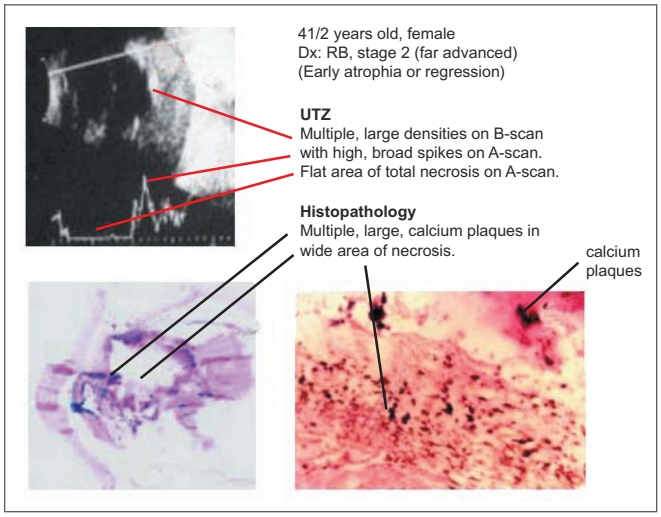

Figure 7. Calcium plaques with necrosis.

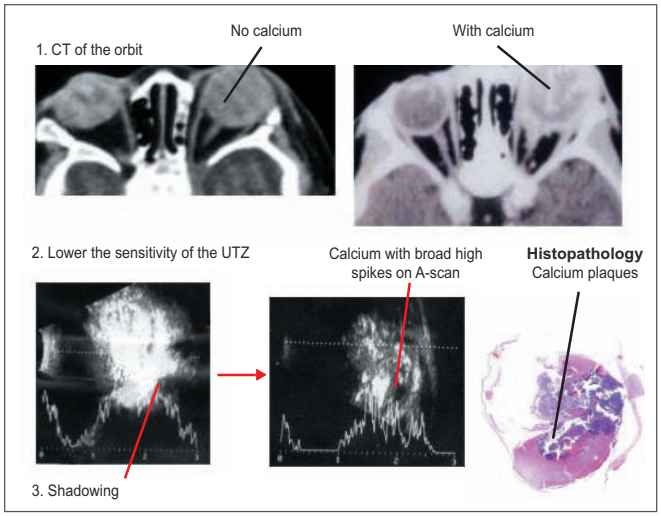

Figure 8. Verification of calcium plaques.

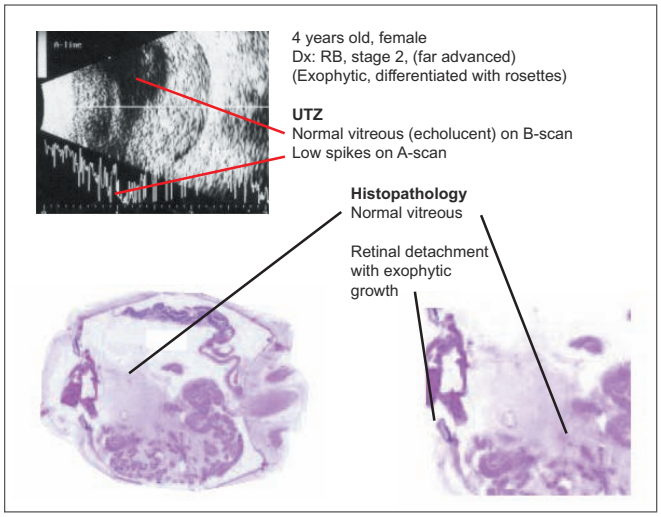

Figure 9. Normal vitreous.

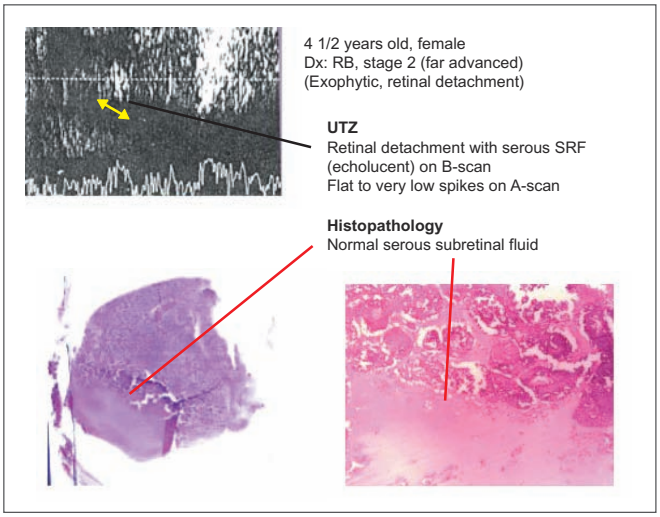

Figure 10. Serous subretinal fluid (SRF).

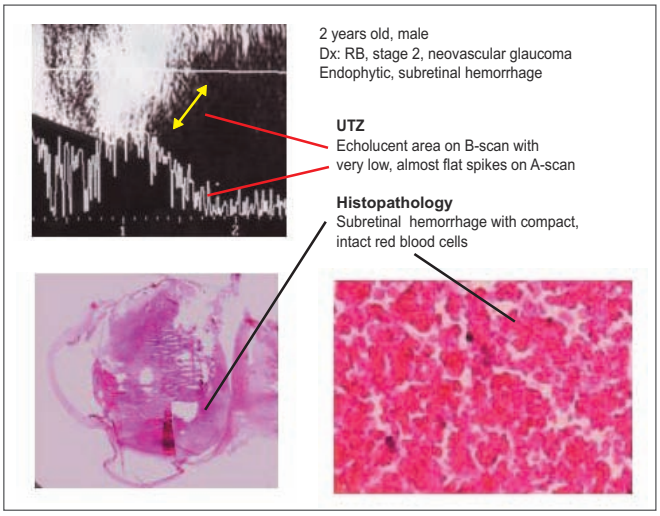

Figure 11. Fresh or recent subretinal hemorrhage.

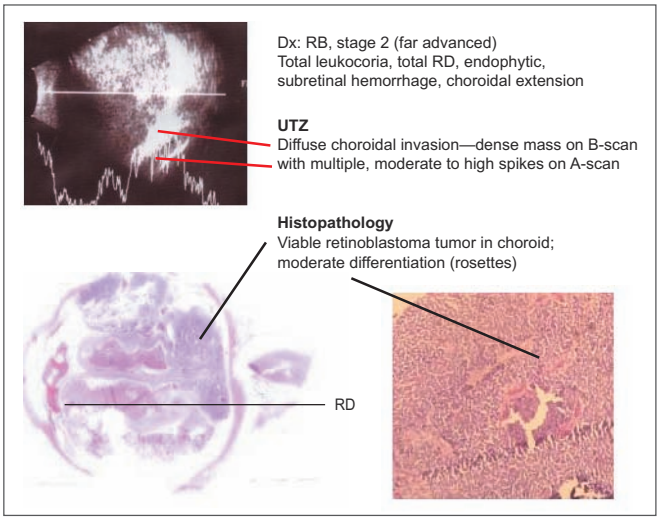

Figure 12. Choroidal extension.

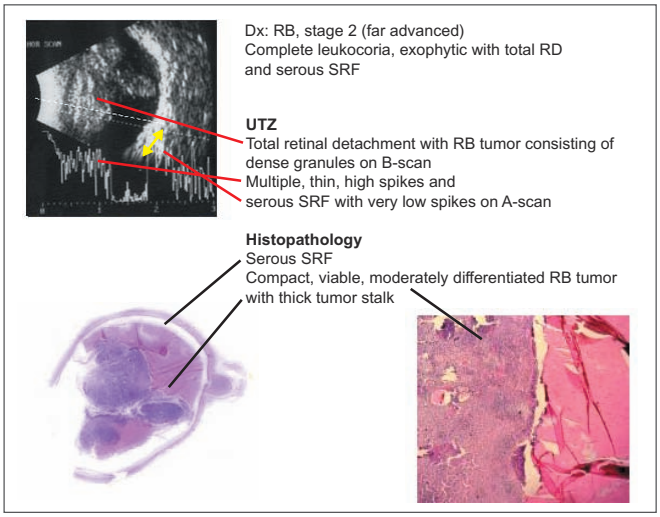

Figure 13. Total RD with RB tumor and serous subretinal fluid.

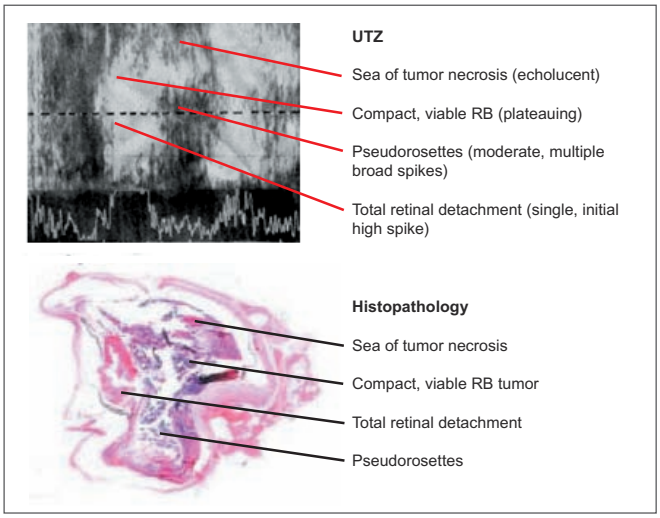

Figure 14. Multiplicity of lesions.

Total RD with RB tumor and serous SRF (Figure 13)

This UTZ pattern is included because it is easily confused preoperatively with nonretinoblastoma intraocular lesions manifesting mainly as leukocoria with a Y-shaped pattern (PHPV, Stage 5 ROP, Coates', Retinal Dysplasia). In retinoblastoma, a total retinal detachment with the stalk attached to the optic disk and the subretinal space filled with serous fluid or hemorrhage is seen. The tumor growth is endophytic toward the vitreous and the stalk is thickened by tumor infiltration. B-scan shows multiple, dense calcium plaques and A-scan shows high internal reflectivity with broad, high spikes corresponding to the calcium plaques. Histopathologic sections show the plaques and the moderately differentiated tumor cells.

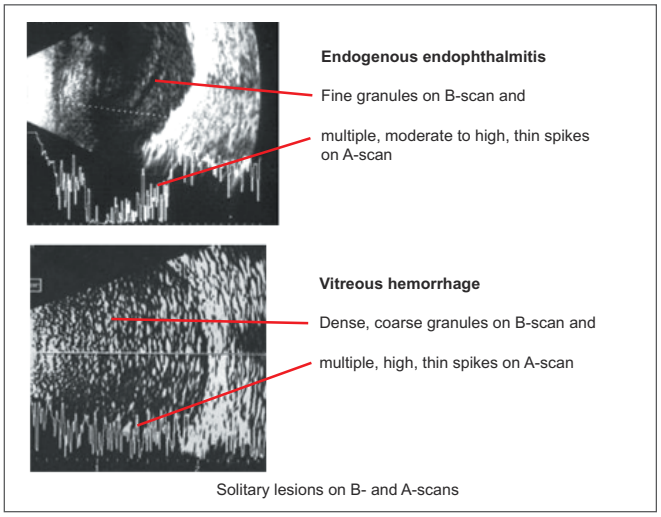

Figure 15. Homogenous lesions (not retinoblastoma).

Multiplicity of lesions (Figure 14)

Often, the multiplicity of lesions gives the diagnosis of retinoblastoma. Called the "Great Mimic" and included among the "Masquerade Syndromes," it exhibits protean manifestations. In Figure 14, UTZ shows echolucent lesions (necrosis), plateauing (compact, well-differentiated, viable RB tumor), short to moderate V-W spikes (pseudorosettes), and a single high spike (detached retina) with corresponding histopathologic lesions. Many intraocular conditions, on the other hand, exhibit single, homogenous lesions (Figure 15).

This study gives the descriptive ultrasound patterns found in retinoblastoma. The incidence of the different patterns cannot be determined because of small sample size, inadequate UTZ work-up, and need for serial histopathologic sections. Future studies should include more samples using more advanced technology (3D ocular sonograph machines that can measure volume and extent and perform coronal sections of the optic-nerve head) and higher–frequency machines (i.e., 30 MHz) with better resolving power.

In summary, ocular UTZ of retinoblastoma shows good histopathologic correlation. The three distinguishing features are calcific plaques with liquefaction necrosis, multiplicity of lesions, and pseudorosettes (Figures 16 and 17). Added information on tumor viability and differentiation will prove valuable in both pre- and postoperative evaluation and therapy.

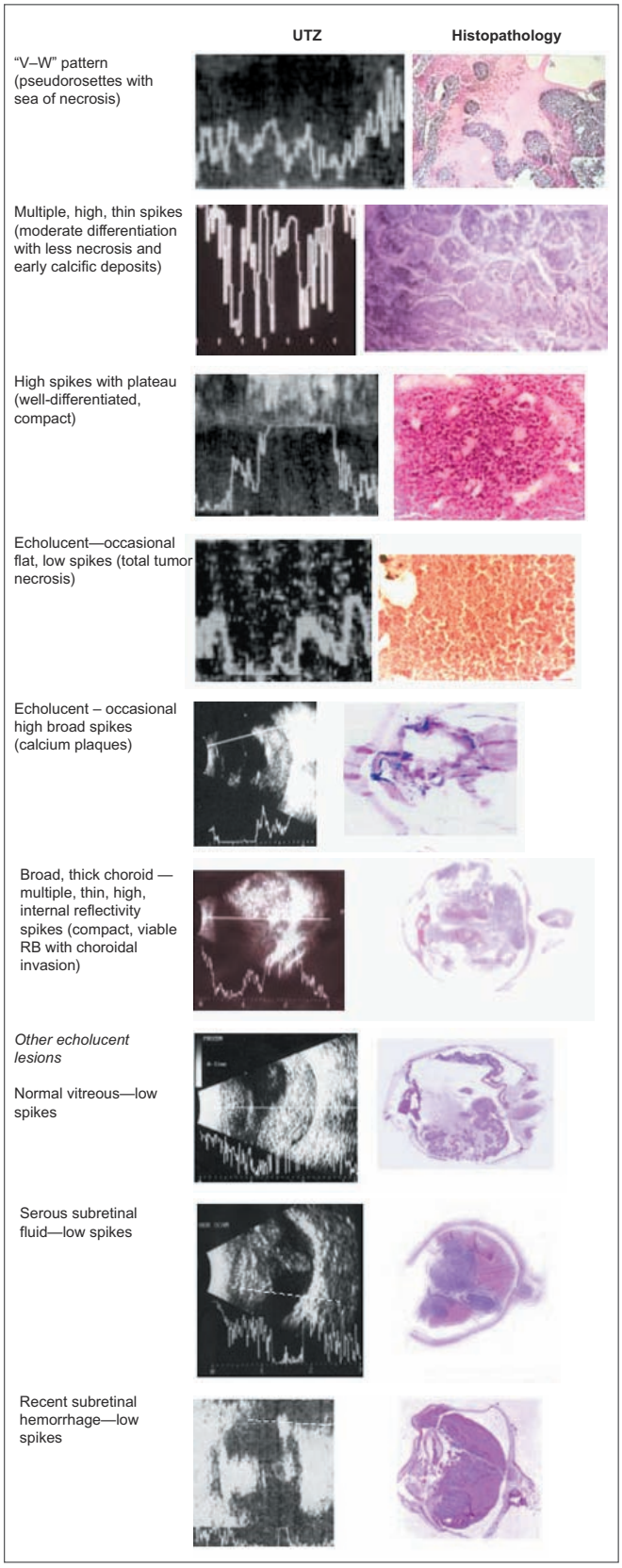

Figure 16. Summary of findings by UTZ and histopathology.

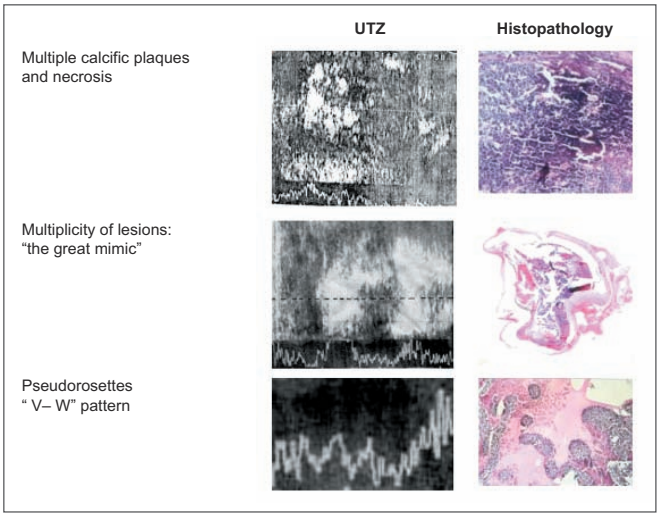

Figure 17. Diagnostic features of retinoblastoma on UTZ.

References

1. Espiritu RB, de Jesus AA, Valera EG, Mercado GV. Epidemiologic pattern of retinoblastoma at the Philippine General Hospital. *Philipp J Ophthalmol* 2005; 3: 136-139.
2. Poujol J, Varene B. Contribution of echography to the diagnosis of retinoblastoma: a homogenous B-scan study. *Ultrasound Med Biol* 1985; 11: 171-175.
3. Zilelioglu G, Gunduz K. Ultrasonic findings in intraocular retinoblastoma and correlation with histopathologic diagnosis. *Int Ophthalmol* 1995; 19: 71-75.
4. Roth DB, Scott IV, Murray TG, et al. Echography of retinoblastoma: histopathologic correlation and serial evaluation after globe-preserving radiotherapy or chemotherapy. *J Ped Ophthalmol Strab* 2001; 38: 136-143.
5. Rykun VS. Computerized ultrasonic diagnosis of voluminous intraocular neoplasms. *Vestn Oftalmol* 2003; 19: 29–31.
6. Bernardino V, Espiritu RB. Retinoblastoma as a cause of enucleation in Filipino children. *Philipp J Med Assn* 1970; 46: 287.
7. Lim G, Torno R. Pathology of eyes enucleated in childhood. *Philipp J Ophthalmol* 1976; 8: 50.
8. Kaste SC, Jenkins JJ III, Pratt CB, et al. Retinoblastoma: sonographic findings with pathologic correlation in pediatric patients. *Am J Radiology* 2000; 175: 495-501.
9. Verma N, Ghose S, Chandrasakhar G. Ultrasonic evaluation of retinoblastoma. *Jpn J Ophthalmol* 1984; 28: 222-229.
10. Byrne SF, Green R. *Textbook on: Ultrasound of the Eye and the Orbit.* St. Louis, MO: Mosby-Year Book, Inc. 1992; 1-15.
11. Koos ML, Nagy I, Koo D. The echographic diagnosis of intraocular tumors in children. *Oftalmologica* 1992; 36: 247-250.
12. Espiritu RB. A modified system of classification of retinoblastoma and its role in diagnosis, therapy, and prognosis. *Philipp J Ophthalmol* 2003; 28: 101-110.

Acknowledgments

The authors gratefully acknowledge the statistical analysis made by Dr. Donna Ma. Santiago and the financial assistance given by United Laboratories, Inc. for the preparation and printing of the colored photographs.